CYCLOGENESIS AND FRONTAL WAVES ON MARS.

J.L. Hollingsworth, *NASA Ames Research Center/SJSUF, Moffett Field, CA 94035 USA (jeffh@humbabe.arc.nasa.gov)*.

Introduction. The atmospheric circulation of Mars reveals similar, yet also very different, features compared to those found on Earth. For example, solar differential heating drives Hadley circulation cells in both atmospheres. However during solstice, Mars' Hadley cells are hemispherically asymmetric: an intense, deep, cross-hemisphere single cell dominates with rising motion in the summer hemisphere and sinking motion in the winter hemisphere. Both planets also exhibit thermally indirect (i.e., eddy-driven) circulation cells in middle and high latitudes. Viking and Mars Global Surveyor (MGS) observations have demonstrated that Mars' winter atmosphere, as Earth's, exhibits traveling weather systems associated with the process of baroclinic instability. Having more regular lifecycles compared to those on Earth [Collins et al., 1996], such traveling disturbances and their poleward transports of heat and momentum, strongly influence the global atmospheric energy budget. An essential aspect of transient baroclinic eddies is that they tend to weaken the baroclinicity of the mean circulation via their associated low-level poleward heat and upper-level momentum fluxes.

Earth and Mars also both exhibit distinctive large-scale orography and, in a broadly defined context, continentality. For Mars' northern midlatitudes, Tharsis in the western hemisphere, and Arabia Terra and Elysium in the eastern hemisphere, are the primary large-scale topographic features. Such underlying orographic complexes not only can cause cause significant latitudinal excursions of the seasonal mean westerly circumpolar flow but also can significantly modulate the intensity and preferred regions of baroclinic weather systems [Hollingsworth et al., 1996; 1997].

Previous numerical modeling studies of baroclinic instability in the Martian atmosphere have mostly applied relatively coarse horizontal resolution. Spectral global circulation models have typically been truncated at T21 (i.e., approximately 5.6° in longitude-latitude) or lower [Collins et al., 1996; Haberle et al., 1997] and grid-point models have had resolutions of $5.0-9.0\times4.0-7.5^\circ$ longitude-latitude [Hourdin et al., 1993; Barnes et al., 1993]. The large-scale, seasonal-mean circulation, as well as dynamical processes intrinsic to the development and decay of the traveling mid- and high-latitude transient baroclinic waves—the synoptic-scale cyclogenesis from which frontal structures may develop—are essentially resolved within the nominal horizontal resolution used by the above mentioned models. However because they are rather coarse (e.g., the smallest horizontal resolved scale in midlatitudes is O(600–800 km)), energy associated with the synoptic scale O(5000 km) cyclogenesis can not adequately cascade into smaller and smaller spatial scales. This precludes fully resolving complex circulations such as shear and stretching deformations accompanying frontal waves on the subsynoptic scale O(1000–2000 km) and less. As such, any abrupt spatial variations within individual dynamical field variables become effectively smeared out.

Over the last couple years, we have been modeling Martian cyclogenesis and frontal waves using fully global circulation models having very high horizontal resolution wherein simulation of traveling baroclinic disturbances is much improved. We report here on the status of this work. Our approach is motivated by Hubble Space Telescope (HST) observations of "comma"-shaped cloud formations and widespread dust activity in the polar region during early northern spring and summer [James et al., 1999]. MGS imaging from the Mars Orbiter Camera (MOC) also indicate large-scale, spiralling condensate cloud structures and scimitar-shaped dust fronts in the polar environment at this season [e.g., James and Cantor, 2001]. Conditions under which surface and/or upper-level fronts (i.e., narrow zones with enhanced mass density, momentum and thermal contrasts within individual transient baroclinic waves) can form in Mars' high-latitude baroclinic zone, and whether associated frontal circulations are sufficient to raise dust in the sub- and extra-tropics can be explored.

Modeling Approach. We have adapted the NASA Goddard Space Flight Center (GSFC) ARIES/GEOS "dynamical core" [Suarez and Takacs, 1995] to Mars' atmosphere. This primitive equations (PE) model integrates the time-dependent equations for the horizontal flow and the thermodynamic energy, as well as imposes constraints of mass conservation and hydrostatic balance for an ideal atmosphere. The vertical coordinate is a normalized pressure, terrain-hugging one (i.e., σ) which enables the lower boundary with spatially-varying topography to coincide with a coordinate surface. The version used conserves energy and mean-square enstrophy, and is fourth-order accurate in terms of vorticity advection by the non-rotational component of the flow. (Currently, this module forms the dynamical processor of the new NASA Ames Research Center Mars general circulation model (GCM), cf. Haberle et al. [2003], this workshop.)

The dynamical configuration we adapt has sixteen unequally-spaced σ layers (denoted L16) with a model "top" pressure of $p_{trop} = 10^{-2}$ mbar (roughly 60 km). Vertical spacing between layers increases from O(500 m) at the surface to O(5 km) in the upper-most part of the model. In the horizontal, we have examined various resolutions, starting with one typically used in the Ames Mars GCM ($7.5^\circ\times9.0^\circ$ longitude-latitude, denoted "G20L16" where the "20" corresponds to half the number of grid points around a latitude circle (also the shortest (Nyquist) resolved spatial scale at the equator). In this work we have also experimented with resolutions

of G75L16, G128L16 and G225L16 (i.e., 2.4° × 2.4°, 1.4° × 1.4°, and, 0.8° × 0.8° longitude-latitude, respectively).

We further apply the global circulation model using simplified physical parameterizations (i.e., an SGCM approach) to mechanistically investigate baroclinic instability within Martian atmosphere at very high horizontal resolution. Diabatic heating is specified in terms of a meridionally dependent thermal relaxation (Newtonian cooling) towards a "radiative equilibrium" temperature field. Upper-level momentum drag is specified in terms of a height-dependent drag (Rayleigh friction), and a simple boundary layer (BL) in terms of drag (i.e., a bulk aerodynamic formulation) via surface stress is imposed in the lowest two layers. The upper-level friction provides an effective "sponge" near the model top so as to inhibit wave reflections caused by the imposed upper-boundary condition (i.e., effectively a rigid lid). The prescribed zonally symmetric radiative equilibrium thermal field as a function of latitude, height and season is independently determined using results from a 1D radiative-convective equilibrium model [Haberle et al., 1997]. To drive the circulation, a diabatic heating term is added to the thermodynamics energy equation of the form

$$\partial T/\partial t = -\alpha_N(\varphi,\sigma)(T - \overline{T}_{eq}(\varphi,\sigma;L_s)) \qquad (1)$$

where $\sigma \equiv (p - p_{trop})/(p_s - p_{trop})$ is the vertical coordinate, p_{trop} is the tropopause pressure, p_s is the surface pressure, and α_N is the thermal damping rate. The height dependent momentum dissipation is imposed in the upper-most three layers of the model by an additional term in the prognostic equations for horizontal momentum

$$\partial(u,v)/\partial t = -\alpha_R(\varphi,\sigma)(u,v) \qquad (2)$$

where $\mathbf{v} = (u,v)$ is the horizontal wind vector and α_R is the dissipation rate. Assuming a neutral BL formulation, we impose

$$\partial(u_b,v_b)/\partial t = -\rho^{-1}(\tau^{(\lambda)},\tau^{(\varphi)})/h \qquad (3)$$

where $(\tau^{(\lambda)},\tau^{(\varphi)}) = \rho C_D|(u_b,v_b)|(u_b,v_b)$, where ρ is the density, C_D is the drag coefficient, $|(u_b,v_b)|$ is the horizontal wind speed in the lowest layers, and h is the layer thickness. For a neutral BL, the drag coefficient is

$$C_D = \left[\frac{0.35}{\ln(z/z_0)}\right]^2 \qquad (4)$$

where z_0 is the surface roughness. In the experiments described subsequently, constant thermal damping and momentum dissipation rates are assumed, and C_D has been set corresponding to mean roughness lengths ranging between 10^{-4} and 10^0 m. Our simulations have focused on integrations centered near northern spring equinox (L_s = 360°) with moderate dust loading (i.e., globally averaged visible optical depth of τ = 0.3–0.5)

Results. The time and zonally-averaged temperature and zonal wind field from a baseline high-resolution (i.e., 2.4 × 2.4° longitude-latitude or G75L16) experiment is shown in Fig. 1. In this experiment, high-resolution Mars topography [e.g., Smith et al., 2001] smoothed to the model's resolution is imposed, and time mean and departure fields have been analyzed from the last 30 days of a 60 day integration. In middle latitudes and aloft, the circulation has adjusted the mean thermal structure significantly different than the prescribed radiative-equilibrium field. Associated with the fairly strong mean north-south temperature gradients are westerly zonal jets which reach speeds of $O(100\,\mathrm{m\,s^{-1}})$. The longitudinal transient wavenumber spectrum at low levels from this experiment is shown in Fig. 2. Both in terms of temperature variance and meridional wind and temperature covariance (i.e., poleward heat flux), the disturbances equilibrate at rather large zonal scales (e.g., s = 1–3) in the middle and high-latitude baroclinic regions, reflecting an overall preferred selection for large-scale transient wave activity and cyclogenesis as has been predicted from coarser model simulations.

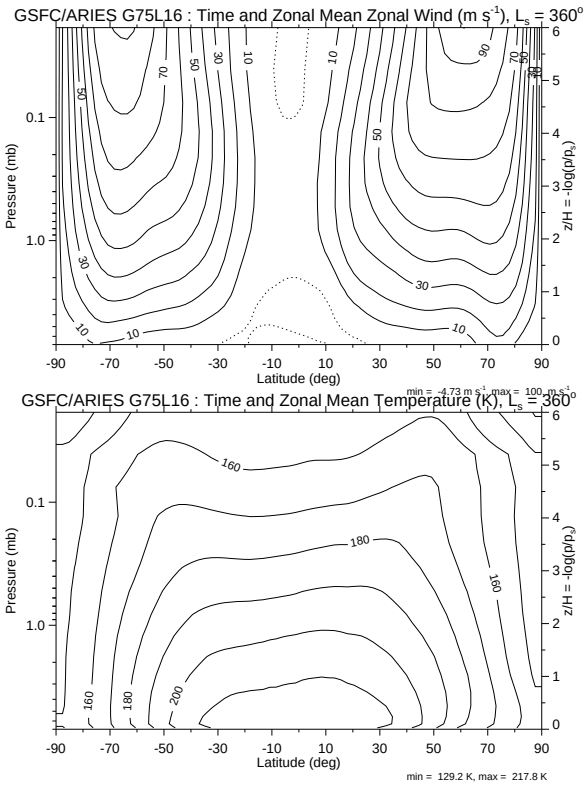

Fig. 1: The time and zonally averaged (a) zonal wind (m s^{-1}) and (b) temperature (K) in the G75L16 experiment with MOLA topography. The contour interval is 10 m s^{-1} and 10 K in (a) and (b), respectively.

Centered at 60°N and the prime meridian, Fig. 3 shows two time snapshots in a spherical projection of the instantaneous surface pressure anomaly (defined as the departure from a 10-day mean, with red indicating

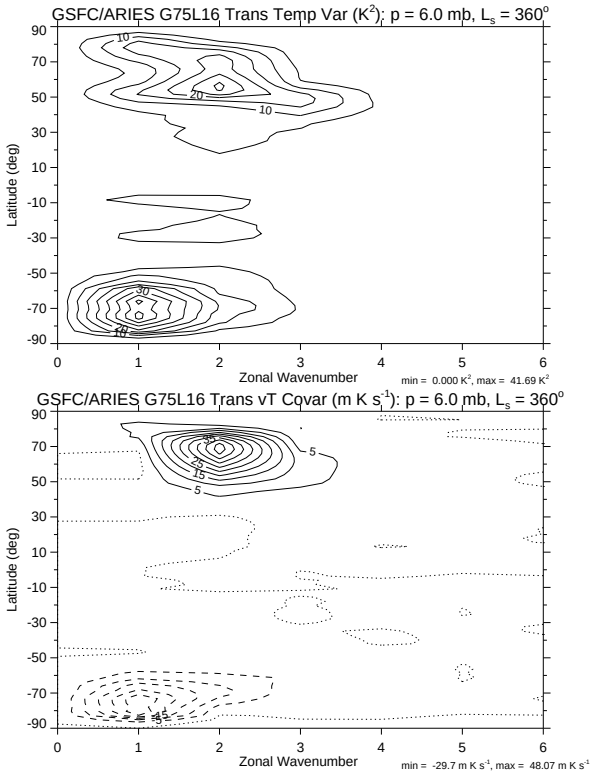

Fig. 2: The transient eddy zonal wavenumber spectrum of (a) temperature variance (K^2) and (b) meridional wind and temperature covariance (m K s^{-1}) at $\sigma = 0.9028$ in the G75L16 experiment with MOLA topography. The contour interval is 5 K^2 and 5 m K s^{-1} in (a) and (b), respectively, and negative values are dashed.

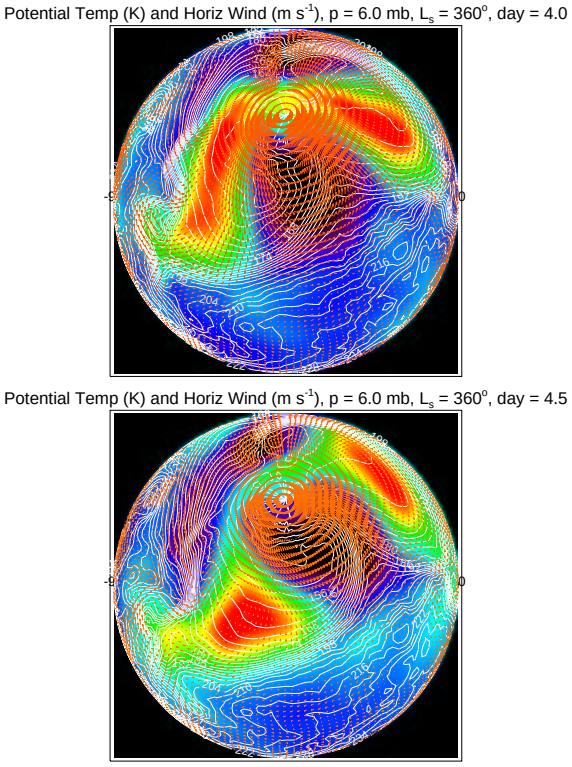

Fig. 3: Spherical projections of potential temperature (K) and horizontal wind (m s^{-1}) at the $\sigma = 0.9028$ surface, and instantaneous surface pressure anomaly (color) on (a) day 4.0 and (b) day 4.5 in the G75L16 experiment with MOLA topography. The temperature contour interval is 3 K.

high pressure and purple/black low pressure), and the potential temperature field at low levels (roughly 6.0 mbar) in the model (indicated by white solid contours). Simulated surface pressure anomaly amplitudes are quite intense, ranging between O(5–10%) from a global reference value (e.g., 7 mbar), which by terrestrial standards, would correspond to near hurricane central pressures. On day 3.0 (not shown), an area of low surface pressure enters the region just to the northeast of Tharsis, which develops into an intense low-pressure system in the Acidalia region within the subsequent twelve hours. By day 4.0, the cyclone and associated frontal wave is highly developed and extends well into the subtropics, with the center of low pressure located near (0°E, 75°N). A significantly cold thermal anomaly O(150 K) associated with the system is found just to the southwest. It can be seen that definite stretching and deformation of the low-level thermal field associated with the surface low and high pressure anomalies occur.

For the same thermal relaxation time scale and imposed surface roughness, the sharpness and horizontal scale of the intense thermal dilation is quite similar in our simulations at higher resolution (e.g., G128L16 and G225L16). That this is the case appears to be related to the large-scale, intense subtropical anticyclone that rapidly develops just to the east of the Tharsis highlands which accentuates the thermal gradient along the axis of contraction of the baroclinic disturbance. In fact, the thermal field shows very tight horizontal gradients and the horizontal wind field is quite complex (e.g., southwesterly flow ahead of the cold air and northwesterly flow behind, with distinct horizontal shear at the gradient boundary). Such flow patterns resemble terrestrial cold fronts. However, with a smaller planetary radius yet similar Rossby deformation scales, the Martian weather systems appear more *hemispherically effective* at "stirring" and "mixing" the high-latitude cold air boundary (i.e., the polar front) well into the midlatitudes and subtropics.

Fig. 4 shows longitude-pressure cross sections of the potential temperature and vertical velocity fields on day 4.5 of the simulation. At the northern latitude circle, the cold frontal surface centered near 60°E appears rather deep, O(5–8 km), and slopes slightly westward with altitude. At the southern latitude circle, a surface-based cold front centered near 45°E appears which is

much shallower, O(3 km), and just to the west, an upper-level cold front appears slightly disconnected from this surface cold front. In both cross sections, clear warm fronts emanate upward less steeply to the east of the cold fronts. The full 3D flow field is spatially complex, with strong upward and down secondary (ageostrophic) motions ahead of and behind the cold frontal boundaries, respectively, which are more intense, O(10–15 cm s^{-1}) at the higher latitude nearer to the cyclone's center. Associated with the strong anticyclone in the western hemisphere, weaker, O(5 cm s^{-1}) subsidence can be seen.

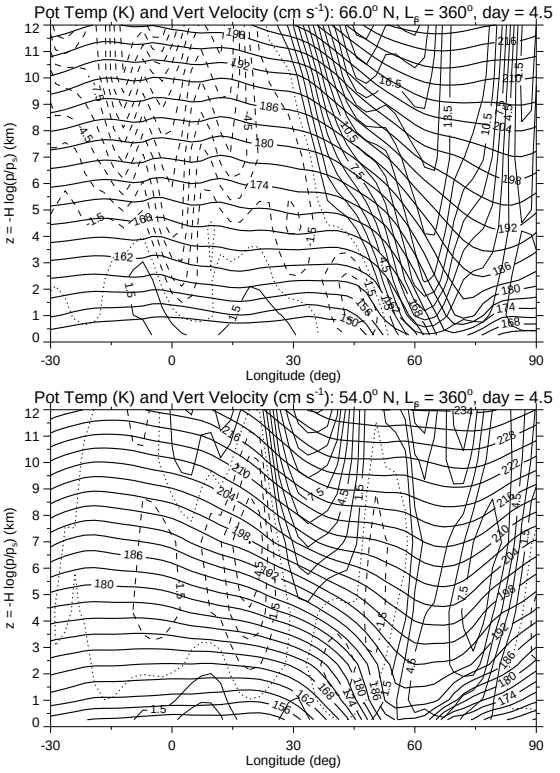

Fig. 4: Longitude-pressure cross section of potential temperature (K) and vertical velocity wind (cm s^{-1}) at 66°N and 54°N on day 4.5 in the G75L16 experiment with MOLA topography. The contour interval is 3 K and 1.5 cm s^{-1} for temperature and vertical velocity, respectively. Negative (descending) values of velocity are dashed, and the zero value is dotted.

In our high resolution simulations that utilize MGS topography, a preference has been found for intensification of the weather systems in the northern low-relief regions (Acidalia, Utopia and Arcadia)—regions identified as "storm zones" using coarser resolution global circulation models [Hollingsworth et al., 1996; 1997]. In addition, clear cold-air and warm-air sectors develop associated with the transient surface pressure anomalies, and distinct "λ"-like signatures in the low-level thermal field can form. These frontal wave structures are the low-level impressions of traveling, amplifying and decaying baroclinic waves. However, in high resolution simulations using flat topography and the same forcing and dissipation prescriptions (not shown), even though strong cyclogenesis and accompanying frontal waves do develop and decay, the transient disturbances exhibit much smaller meridional scales, which results in the strongest thermal gradients and horizontal flow convergence developing polewards of 40–50°N. Orography appears to play a significant role in breaking the hemispheric symmetry of the Martian northern cold polar front, and in so doing, determining the character and meridional scale of the individual baroclinic waves and the accompanying frontal disturbances.

Summary and Conclusions. High resolution, mechanistic global circulation modeling (full PE) can simulate subsynoptic scale O(700–2000 km) frontogenesis in Mars' atmosphere, i.e., a focused energy cascade from the synoptic-scale O(5000 km) cyclogenesis associated with traveling baroclinic waves. For early northern spring (L_s = 360°), the frontal systems can develop/decay, and progress rapidly (e.g., equatorward and eastward). The frontal waves also exhibit large spatial extents (e.g., reaching from middle and high latitudes in to the subtropics). These systems can effectively distort and "stir" the high-latitude circumpolar cold-air boundary (i.e., the Martian polar front). Furthermore, the most intense frontal systems appear frequently "triggered" from large-scale upstream orography (e.g., the Tharsis ridge) and achieve largest amplitude in low-relief regions (e.g., Acidalia), i.e., within Mars' northern-hemisphere "storm zones" as predicted using low-resolution circulation models. Examination of the details of the frontal wave circulations indicate strong associated secondary (i.e., ageostrophic) circulations at their boundary, with sinking motion behind, rising motion ahead of the sloping frontal surface. Modeling the circulation at high spatial resolution is necessary in order to illuminate processes important to local and regional dust activity, and condensate cloud formation, structure, and evolution within the edge of the seasonal polar caps. Global high-resolution modeling can aid in the assessment of Mars' polar climate, in particular, the intensity of circulation regimes that can develop.

References. Barnes, J.R., et al., 1993: *J. Geophys. Res.,* **98,** 3125–3148; Collins, M., et al., 1996: *Icarus,* **120,** 344–357; Haberle, R.M., et al., 1997: *J. Geophys. Res.,* **102,** 9051–9067; Hollingsworth, J.L., et al., 1996: *Nature,* **102,** 413–416; Hollingsworth, J.L., et al., 1997: *Adv. Space Res.,* **19,** 1237–1240; Hourdin, F., et al., 1993: *J. Atmos. Sci.,* **50,** 3625–3640; James, P.B., et al., 1999: *Icarus,* **138,** 64–73; James, P.B., and B.A. Cantor, 2001: *Icarus,* **154,** 131–144; Suarez, M.J., and L.L. Takacs, 1995: NASA Technical Memorandum 104606, Vol. 5; Smith, D.E., et al., 2001: *J. Geophys. Res.,* **106,** 23689–23722.

Acknowledgements. This research has been supported by a NASA Ames University Cooperative Agreement (NCC2-5336) with San Jose State University.